198520: garnet-bearing orthopyroxene pelitic granofels, Tregenza Road

(Youanmi Terrane, Yilgarn Craton)

Blereau, ER, Korhonen, FJ, Kelsey, DE and Fielding, IOH

Location and sampling

CORRIGIN (SI 50-3), BROOKTON (2333)

MGA Zone 50, 538023E 6442092N

Warox Site FJKBGD198520

Sampled on 2 June 2010

This sample was collected from a dam wall in a paddock, about 8.0 km south of Bugin Rock, 7.6 km southwest of Juropin Rock and 0.2 km north of Tregenza Road. The sample was collected as part of the Geological Survey of Western Australia's (GSWA) 2003–14 Yilgarn Craton Metamorphic Project, and referred to in that study as sample BG10-10b. The results from this project have not been released by GSWA, although select data have been published in Goscombe et al. (2019).

Geological context

The unit sampled is a granulite-grade pelitic granofels near the western margin of the Youanmi Terrane (Quentin de Gromard et al., 2021). The unit is part of a northwest-trending belt of Archean metasedimentary and gneissic rocks referred to by Wilde (2001) and Bosch et al. (1996) as the Jimperding metamorphic belt. The boundary between the South West and Youanmi Terranes in this area is a major, northwest-trending shear zone system (Quentin de Gromard et al., 2021). A second sample of pelitic granofels was also collected from this locality (GSWA 198522). Four quartzite samples, collected between 99 and 111 km northwest of this locality, yielded detrital zircon ages between c. 3700 and 3000 Ma, and maximum ages of deposition between c. 3203 and 3005 Ma (GSWA 177901, Wingate et al., 2008a; GSWA 177904, Wingate et al., 2008b; GSWA 177907, Wingate et al., 2008c; GSWA 177908, Wingate et al., 2008d; Pidgeon et al., 2010). Zircon rims in two of these samples have been interpreted to date amphibolite facies metamorphism at c. 2660 Ma (GSWA 177907, Wingate et al., 2008c; GSWA 177908, Wingate et al., 2008d). Monazite from a pelitic gneiss about 21 km to the west-southwest yielded a weighted mean $^{207}Pb/^{206}Pb$ date of 2647 ± 5 Ma, interpreted as the age of high-grade metamorphism (GSWA 198516, Fielding et al., 2021c). Monazite from the sample reported here yielded a weighted mean $^{207}Pb/^{206}Pb$ date of 2651 ± 6 Ma, interpreted as the age of high-grade metamorphism (GSWA 198520, Fielding et al, 2021a). The second sample collected from this locality yielded a similar monazite age of 2656 ± 6 Ma (GSWA 198522, Fielding et al, 2021b). A summary of the metamorphic evolution of the southwest Yilgarn Craton is provided in Korhonen et al. (2021).

Petrographic description

The sample is a weakly foliated, medium-grained Fe-rich pelitic granofels containing about 37% orthopyroxene, 24% plagioclase, 22% biotite, 9% K-feldspar, 4% garnet, 3% quartz, 1% magnetite, and trace amounts of ilmenite, monazite and zircon (Fig. 1; Table 1). The sample has subtle cm-scale layering defined by a higher proportion of garnet and plagioclase alternating with domains that have a higher abundance of orthopyroxene, biotite, and K-feldspar (Figs 1, 2a). Orthopyroxene is Al-rich and forms weakly elongate anhedral grains up to 1.5 mm in size with pink–green pleochroism (Fig. 2b) in the matrix and as inclusions in garnet (Figs 1, 2c). Smaller orthopyroxene grains up to 0.5 mm in size are dispersed in plagioclase-rich layers. Feldspars are fresh and unaltered, with plagioclase forming small rounded grains up to 1 mm in size (Fig. 2a–c), and K-feldspar occurring as larger crystals up to 3 mm in size (Fig. 2b). There is also rare myrmekite in orthopyroxene-rich layers. Laths of red to orange biotite up to 1.5 mm long

define a weak foliation (Fig. 1) that is closely associated with orthopyroxene (Fig. 2), and also occurs as inclusions in garnet (Fig. 2a,c). Garnet occurs as irregularly shaped anhedral porphyroblasts up to 4 mm in diameter that host rounded inclusions of biotite, orthopyroxene, ilmenite, quartz, plagioclase and K-feldspar (Figs 1, 2c). Garnet porphyroblasts are almandine-rich with no significant compositional zoning in Fe, Mn and Ca, and a very slight decrease in Mg at the outermost rim (Appendix). Quartz forms anhedral grains less than 0.5 mm in size and occurs interstitially with all minerals, as minor intergrowths with plagioclase, as inclusions in garnet, and as rare moats around magnetite. Magnetite and ilmenite occur as small disseminated grains throughout the matrix. This granulite-facies granofels was likely derived from a Fe-rich pelitic metasedimentary protolith.

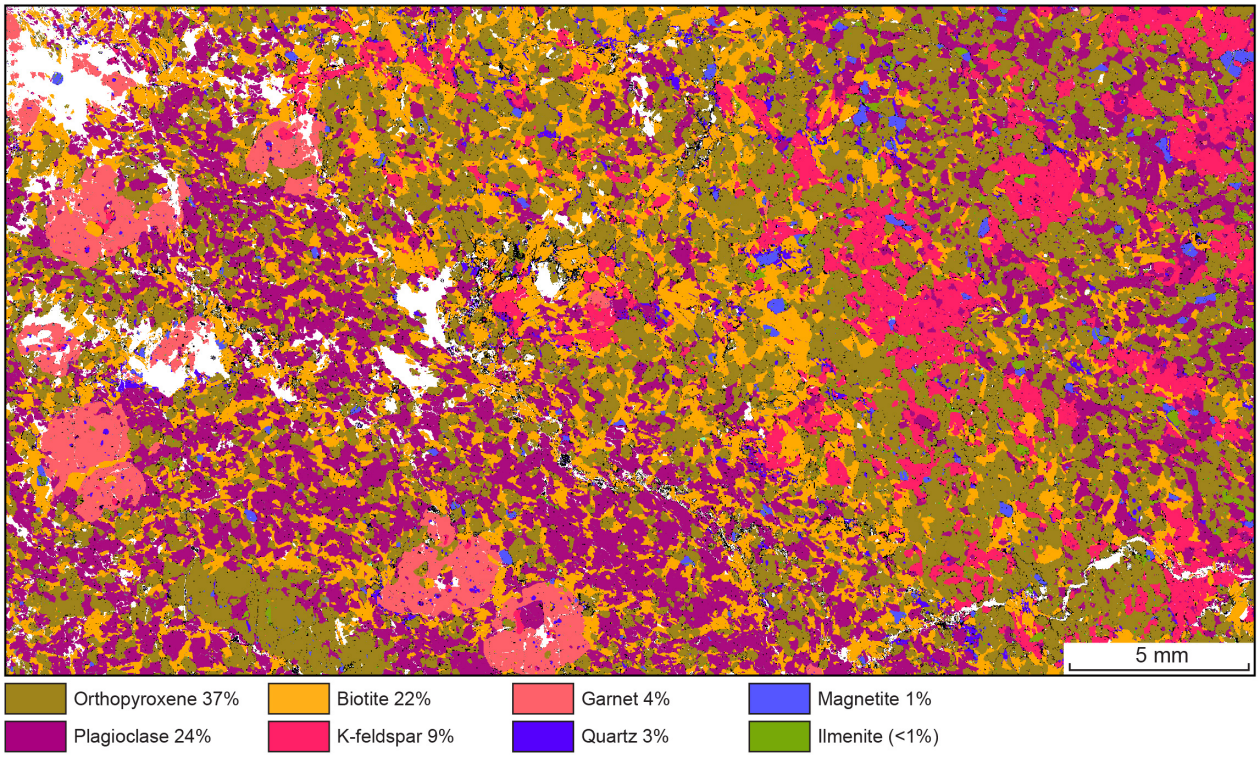

Figure 1. **TESCAN Integrated Mineral Analyser (TIMA) image of an entire thin section from sample 198520: garnet-bearing orthopyroxene pelitic granofels, Tregenza Road. Volume percent proportions of major rock-forming minerals are calculated by the TIMA software**

Table 1. Mineral modes for sample 198520: garnet-bearing orthopyroxene pelitic granofels, Tregenza Road

Mineral modes	*Pl*	*Bt*	*Grt*	*Qz*	*Kfs*	*Ap*	*Mag*	*Ilm*	*Opx*
Observed (vol%)	4	37	22	24	9	3	trace	1	–
Predicted (mol%)									
@ 6.6 kbar, 845 °C	6	33	7	37	9	–	3	1	3
@ 6.6 kbar, 960 °C	0.1	38	4	35	10	–	2	3	8

NOTES: – not present

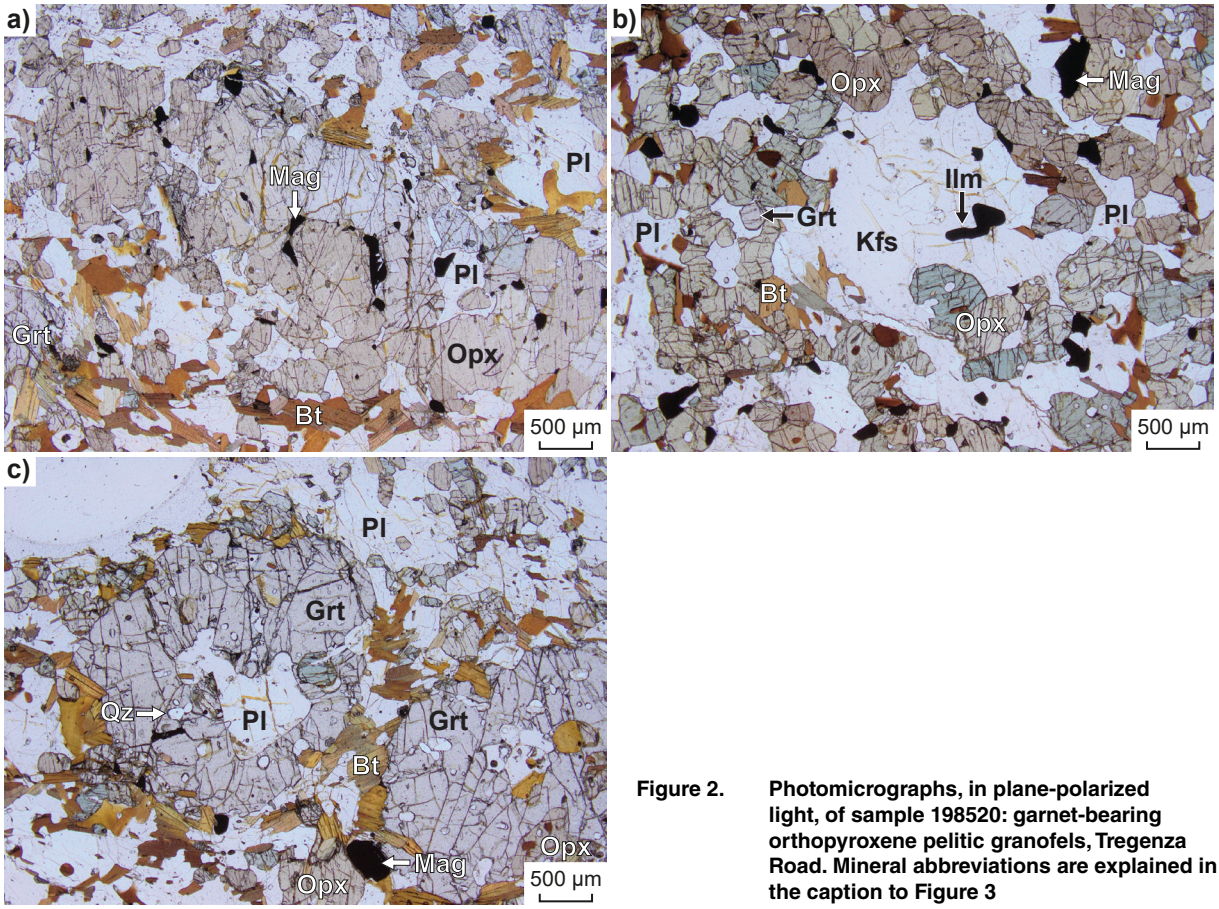

Figure 2. **Photomicrographs, in plane-polarized light, of sample 198520: garnet-bearing orthopyroxene pelitic granofels, Tregenza Road. Mineral abbreviations are explained in the caption to Figure 3**

Analytical details

Preliminary *P–T* estimates were obtained using multiple-reaction thermobarometry calculated from the mineral compositions (Table 2; Goscombe et al., 2019). These estimates were derived from the 'averagePT' module (avPT) in the program THERMOCALC version tc325 (Powell and Holland, 1988), using the internally consistent Holland and Powell (1998) dataset.

The metamorphic evolution of this sample has subsequently been re-evaluated using phase equilibria modelling, based on the bulk-rock composition (Table 3). The bulk-rock composition was determined by X-ray fluorescence spectroscopy, together with loss on ignition (LOI). FeO content was analysed by Fe^{2+} titration, and Fe_2O_3 calculated by difference. The modelled O content (for Fe^{3+}) was derived from the titration value. The appropriate H_2O content for the *P–T* pseudosection was evaluated using a *T*–M_{H2O} pseudosection (not shown), extending from a nominally anhydrous composition (M_{H2O} = 0; 0.01 mol%) to the measured LOI value (M_{H2O} = 1; 2.91 mol%). An appropriate H_2O content should ideally reproduce the observed mineral assemblage in approximately the same proportions at conditions just below the solidus. Using this criteria, a M_{H2O} value of 0.4 (= 1.17 mol%) was selected for the bulk composition to calculate the *P–T* pseudosection. The bulk composition was also adjusted for the presence of apatite by applying a correction to CaO (Table 3). Thermodynamic calculations were performed in the MnNCKFMASHTO ($MnO–Na_2O–CaO–K_2O–FeO–MgO–Al_2O_3–SiO_2–H_2O–TiO_2–O$) system using THERMOCALC version tc340 (updated October 2013; Powell and Holland, 1988) and the internally consistent thermodynamic dataset of Holland and Powell (2011; dataset tc-ds62, created in February 2012). The activity–composition relations used in the modelling are detailed in White et al. (2014a,b). Compositional and mode isopleths for all phases were calculated using the software TCInvestigator (Pearce et al., 2015). Additional information on the workflow with relevant background and methodology are provided in Korhonen et al. (2020).

Table 2. Mineral compositions for sample 198520: garnet-bearing orthopyroxene pelitic granofels, Tregenza Road

Mineral[(a)]	*Bt*	*Opx*	*Ilm*	*Grt*	*Grt*	*Grt*	*Grt*	*Grt*	*Kfs*	*Kfs*	*Opx*	*Opx*	*Bt*	*Bt*
Setting[(b)]	*Incl*	*Incl*	*Incl*	*Core*	*Mantle*	*Mantle*	*Rim*	*OR*	*Core*	*Rim*	*Core*	*Rim*	*Core*	*Rim*
wt%														
SiO_2	36.91	49.56	0.02	37.95	38.63	38.12	37.74	38.78	59.79	60.06	49.22	49.24	36.20	36.23
TiO_2	5.95	0.11	47.83	0.00	0.05	0.05	0.06	0.01	0.00	0.00	0.13	0.11	5.70	5.45
Al_2O_3	15.32	4.88	0.00	21.55	21.63	21.28	21.20	21.49	25.10	25.29	4.54	4.65	15.38	15.59
Cr_2O_3	0.05	0.03	0.05	0.00	0.01	0.03	0.03	0.00	0.03	0.00	0.01	0.02	0.05	0.06
FeO	13.42	24.78	46.20	28.43	27.92	30.47	30.75	28.59	0.04	0.32	26.41	26.39	16.23	16.05
MnO	0.01	0.65	2.21	2.52	2.43	2.59	2.59	2.62	0.01	0.01	0.77	0.78	0.10	0.10
MgO	14.62	19.89	0.03	7.99	7.72	6.29	5.79	7.70	0.00	0.00	18.60	18.62	12.25	12.37
ZnO	0.07	0.05	0.00	0.08	0.00	0.04	0.01	0.10	0.08	0.03	0.01	0.02	0.00	0.00
CaO	0.00	0.18	0.01	1.47	1.53	1.38	1.31	1.48	7.80	7.37	0.13	0.13	0.00	0.02
Na_2O	0.22	0.01	0.00	0.00	0.00	0.02	0.02	0.05	7.28	7.22	0.00	0.03	0.11	0.16
K_2O	9.58	0.02	0.00	0.00	0.02	0.04	0.06	0.00	0.43	0.32	0.00	0.02	9.62	9.79
Total[(c)]	96.15	100.15	96.36	99.99	99.93	100.29	99.57	100.81	100.57	100.62	99.81	99.99	95.64	95.83
Oxygen	11	6	3	12	12	12	12	12	8	8	6	6	11	11
Si	2.71	1.86	0.00	2.95	3.01	2.99	2.99	3.00	2.66	2.67	1.87	1.87	2.71	2.71
Ti	0.33	0.00	0.94	0.00	0.00	0.00	0.00	0.00	0.00	0.00	0.00	0.00	0.32	0.31
Al	1.33	0.22	0.00	1.98	1.98	1.97	1.98	1.96	1.31	1.32	0.20	0.21	1.36	1.38
Cr	0.00	0.00	0.00	0.00	0.00	0.00	0.00	0.00	0.00	0.00	0.00	0.00	0.00	0.00
Fe^{3+}[(d)]	0.04	0.06	0.12	0.12	0.00	0.04	0.03	0.05	0.00	0.00	0.05	0.06	0.05	0.05
Fe^{2+}	0.78	0.72	0.89	1.73	1.82	1.96	2.01	1.80	0.00	0.01	0.79	0.78	0.97	0.95
Mn^{2+}	0.00	0.02	0.05	0.17	0.16	0.17	0.17	0.17	0.00	0.00	0.02	0.02	0.01	0.01
Mg	1.60	1.11	0.00	0.93	0.90	0.74	0.68	0.89	0.00	0.00	1.05	1.05	1.37	1.38
Zn	0.00	0.00	0.00	0.00	0.00	0.00	0.00	0.01	0.00	0.00	0.00	0.00	0.00	0.00
Ca	0.00	0.01	0.00	0.12	0.13	0.12	0.11	0.12	0.37	0.35	0.01	0.01	0.00	0.00
Na	0.03	0.00	0.00	0.00	0.00	0.00	0.00	0.01	0.63	0.62	0.00	0.00	0.02	0.02
K	0.90	0.00	0.00	0.00	0.00	0.00	0.01	0.00	0.02	0.02	0.00	0.00	0.92	0.93
Total	5.00	5.00	5.00	5.00	8.00	8.00	8.00	7.60	7.59	7.61	4.00	4.00	4.00	2.00
Compositional variables[(e)]														
y(Opx)	–	–	–	–	–	–	–	–	–	–	0.07	0.07	–	–
XFe	0.33	0.39	–	0.65	0.67	0.73	0.75	0.67	–	–	0.43	0.43	0.41	0.41

NOTES: – not applicable
(a) Mineral abbreviations explained in the caption to Figure 3
(b) Incl, inclusion; OR, outer rim
(c) Totals on anhydrous basis
(d) Fe^{3+} contents for biotite assumed to be 10% of Fe total; Fe^{3+} contents for other minerals based on Droop (1987)
(e) *y*(Opx) = Al on the M1 site; White et al. (2014a); XFe = $Fe^{2+}/(Fe^{2+} + Mg)$

Table 3. Measured whole-rock and modelled compositions for sample 198520: garnet-bearing orthopyroxene pelitic granofels, Tregenza Road

XRF whole-rock composition (wt%)[(a)]

SiO_2	**TiO_2**	**Al_2O_3**	**Fe_2O_3[(b)]**	**FeO[(b)]**	**MnO**	**MgO**	**CaO**	**Na_2O**	**K_2O**	**P_2O_5**	**LOI**	**Total**
49.36	1.54	14.97	3.88	12.20	0.41	8.05	3.00	2.62	2.28	0.21	<0.01	98.52

Normalized composition used for phase equilibria modelling (mol%)

SiO_2	**TiO_2**	**Al_2O_3**	**O[(c)]**	**FeO^T[(d)]**	**MnO**	**MgO**	**CaO[(d)]**	**Na_2O**	**K_2O**	**–**	**H_2O[(e)]**	**Total**
52.18	1.22	9.32	1.55	13.87	0.37	12.69	3.40	2.69	1.54	--	1.17	100

NOTES: (a) Data and analytical details are available from the WACHEM database <http://geochem.dmp.wa.gov.au/geochem/>
(b) FeO analysed by Fe^{2+} titration; Fe_2O_3 content calculated by difference
(c) O content (for Fe_2O_3) based on titration value
(d) CaO modified to remove apatite: CaO(Mod) = CaO(Total) - (moles CaO(in Ap) = 3.33 * moles P_2O_5)
(e) H_2O content based on T–M_{H2O} diagram; see text for additional details

Results

Metamorphic *P–T* estimates have been derived based on detailed examination of two thin sections and the bulk-rock composition; care was taken to ensure that the thin section and the sample volume selected for whole-rock chemistry were similar in terms of featuring the same minerals in approximately the same abundances (Table 1), to minimize any potential compositional differences. The *P–T* pseudosection was calculated over a *P–T* range of 2–10 kbar and 750–1000 °C (Fig. 3). The solidus is located between 790 and 870 °C across the range of modelled pressures, with quartz-absent assemblages stable at temperatures just above the solidus. Magnetite is stable up to 7.7 kbar, with garnet-absent assemblages stable below 6.5 kbar at 1000 °C and 4 kbar at 750 °C. Cordierite has a maximum pressure stability of 4 kbar between 750 and 865 °C, and decreases below 2 kbar at temperatures above 865 °C.

Metamorphic *P–T* estimates (± 2σ uncertainty) calculated using multiple-reaction thermobarometry are 6.0 ± 1.1 kbar and 814 ± 76 °C (Goscombe et al., 2019). These calculations used the core compositions (Table 2) to estimate peak conditions.

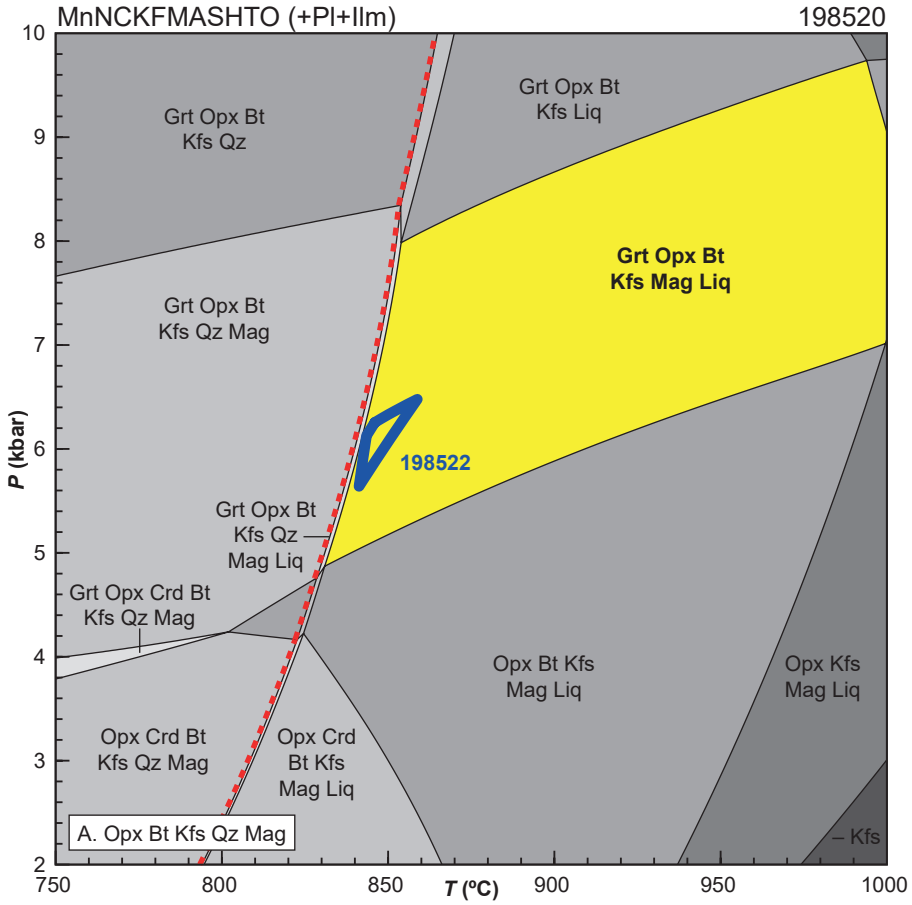

Figure 3. ***P–T*** **pseudosection calculated for sample 198520: garnet-bearing orthopyroxene pelitic granofels, Tregenza Road. Assemblage fields corresponding to peak metamorphic conditions are shown in bold text and yellow shading. Red dashed line represents the solidus. Blue field corresponds to peak *P–T* estimates from a sample collected from the same locality (GSWA 198522, Blereau et al., 2022). Thick blue lines show the region of overlap between the two samples, which is the best estimate for peak conditions. Abbreviations: Bt, biotite; Crd, cordierite; Grt, garnet; Ilm, ilmenite; Kfs, K-feldspar; Liq, silicate melt; Mag, magnetite; Opx, orthopyroxene; Pl, plagioclase; Qz, quartz**

Interpretation

Based on the coarser grain size and mineral associations that support textural equilibrium, the peak granulite-grade metamorphic assemblage is interpreted to be garnet–orthopyroxene–biotite–plagioclase–K-feldspar–ilmenite–magnetite–melt±quartz. There is uncertainty on whether the sparse interstitial quartz is part of the peak assemblage or a retrograde phase. Inclusions of orthopyroxene are preserved in garnet, whereas inclusions of garnet are not observed in orthopyroxene. This relationship suggests that some orthopyroxene growth may have pre-dated at least some garnet growth, although the possibility that orthopyroxene inclusions were in equilibrium with the garnet host cannot be ruled out.

The inferred peak assemblage of garnet–orthopyroxene–biotite–plagioclase–K-feldspar–ilmenite–magnetite–melt is stable between 830 and 1000 °C at 4.9 – 9.7 kbar, with the quartz-bearing assemblage stable in a very narrow field at the solidus at slightly lower temperatures of 825–855 °C at 4.8 – 8.3 kbar. The predicted mineral modes (molar proportions approximately equivalent to vol%) across the peak field at 6.6 kbar are broadly similar to the modes observed in the thin section (Table 1). The amount of biotite and plagioclase predicted in the modelling are lower and higher, respectively, to the amounts observed in the thin section (Table 1). Some retrograde growth of biotite following melt crystallization could account for the increase in biotite. Modal isopleths for orthopyroxene and garnet have relatively shallow slopes across the peak field, and garnet growth at the expense of orthopyroxene is most consistent with an increase in pressure (Fig. 4a,b). The inferred sequence of mineral growth consisting of orthopyroxene, followed by garnet growth at the expense of orthopyroxene, and the growth of retrograde quartz at conditions near the solidus is broadly consistent with an anticlockwise *P–T* path (Fig. 4a–c).

Peak metamorphic conditions are estimated at 830–1000 °C and 4.9 – 9.7 kbar. These estimates can be refined using the Al content in orthopyroxene, which can retain its peak composition under high temperature conditions (e.g. Fitzsimons and Harley, 1994; Pattison et al., 2003). Orthopyroxene porphyroblasts preserve Al contents (on the M1 site = y(Opx)) of 0.07 (Table 2). Comparing the observed orthopyroxene compositions with the values predicted on the *P–T* pseudosection (Fig. 4d, green-shaded band) refine conditions in the inferred peak field to pressures above 6.5 kbar. A sample collected from the same locality yields peak *P–T* estimates of 5.6 – 6.5 kbar and 845–860 °C (GSWA 198522, Blereau et al., 2022). The *P–T* constraints from sample GSWA 198522 fall within the peak field for the sample reported here, and provide the best estimate for peak conditions (Fig. 3). The predicted y(Opx) values in the area of overlap are slightly higher than the measured values, but these compositions could record the conditions of melt crystallization and preservation of the observed assemblage after crossing the high-temperature solidus at about 6.5 kbar (Fig. 4d), which is also suggestive of an anticlockwise *P–T* path.

Based on the results of two samples from the same locality with similar metamorphic ages, peak metamorphic conditions are estimated at 5.6 – 6.5 kbar and 845–860 °C, with an apparent thermal gradient of approximately 130–150 °C/kbar. The growth of garnet at the expense of orthopyroxene, retrograde growth of quartz, and orthopyroxene compositions broadly support an anticlockwise *P–T* path, with final melt crystallization at 850 °C and 6.5 kbar.

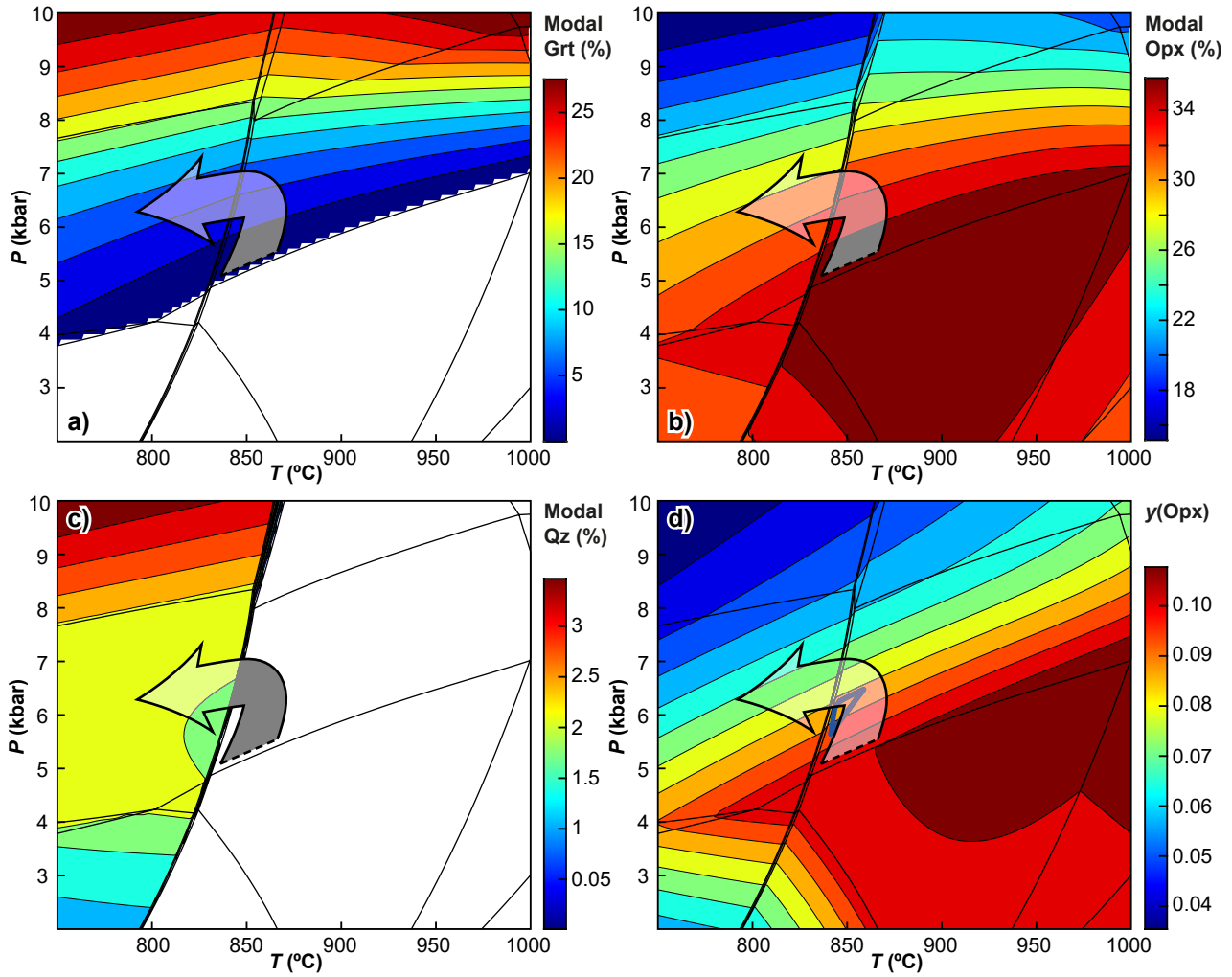

Figure 4. ***P–T*** **pseudosections with calculated isopleths: a–c) mode isopleths (mineral proportions; approximately equal to volume percent) for selected minerals in sample 198520: garnet-bearing orthopyroxene pelitic granofels, Tregenza Road (see Figure 3 for labelled *P–T* diagram); d) compositional isopleths of Al contents in orthopyroxene (on the M1 site = *y*(Opx)). Thick blue lines outline the peak *P–T* estimates constrained from this locality (see Fig. 3). The growth of garnet after orthopyroxene, retrograde growth of quartz, and measured y(Opx) values of 0.07 broadly support an anticlockwise trajectory; schematic *P–T* path is represented by the grey arrow at the minimum temperatures within the area of overlap, with thickness of the arrow to qualitatively depict uncertainty**

References

Blereau, ER, Korhonen, FJ, Fielding, IOH and Kelsey DE 2022, 198522: orthopyroxene–garnet–cordierite pelitic granofels, Tregenza Road; Metamorphic History Record 15: Geological Survey of Western Australia, 8p.

Bosch, D, Bruguier, O and Pidgeon, RT 1996, Evolution of an Archean metamorphic belt: A conventional and SHRIMP U–Pb study of accessory minerals from the Jimperding metamorphic belt, Yilgarn Craton, Western Australia: The Journal of Geology, v. 104, p. 695–711.

Droop, GTR 1987, A general equation for estimating Fe^{3+} concentrations in ferromagnesian silicates and oxides from microprobe analyses, using stoichiometric criteria: Mineralogical Magazine, v. 51, no. 361, p. 431–435, <https://doi.org/10.1180/minmag.1987.051.361.10>.

Fielding, IOH, Wingate, MTD, Korhonen, FJ and Rankenburg, K 2021a, 198520: pelitic granofels, Tregenza Road; Geochronology Record 1765: Geological Survey of Western Australia, 5p.

Fielding, IOH, Wingate, MTD, Korhonen, FJ and Rankenburg, K, 2021b; 198522: pelitic granofels, Tregenza Road; Geochron Record 1766: Geological Survey of Western Australia, 5p.

Fielding, IOH, Wingate, MTD, Korhonen, FJ and Rankenburg, K 2021c, 198516: pelitic granofels, Quajabin Peak; Geochronology Record 1764: Geological Survey of Western Australia, 5p.

Fitzsimons, ICW and Harley, SL 1994, The Influence of Retrograde Cation Exchange on Granulite P–T Estimates and a Convergence Technique for the Recovery of Peak Metamorphic Conditions: Journal of Petrology, v. 35, no. 2, p. 543–576.

Goscombe, B, Blewett, R, Groenewald, PB, Foster, D, Wade, B, Wyche, S, Wingate, MTD and Kirkland, CL 2015, Metamorphic Evolution of the Yilgarn Craton: Geological Survey of Western Australia (unpublished), 910p.

Goscombe, B, Foster, DA, Blewett, R, Czarnota, K, Wade, B, Groenewald, B and Gray, D 2019, Neoarchaean metamorphic evolution of the Yilgarn Craton: a record of subduction, accretion, extension and lithospheric delamination: Precambrian Research, article no. 105441, doi:10.1016/j.precamres.2019.105441, <https://www.sciencedirect.com/science/article/pii/S0301926818305588>.

Holland, TJB and Powell, R 2011, An improved and extended internally consistent thermodynamic dataset for phases of petrological interest, involving a new equation of state for solids: Journal of Metamorphic Geology, v. 29, no. 3, p. 333–383.

Korhonen, FJ, Blereau, ER, Kelsey, DE, Fielding, IOH and Romano, SS 2021, Metamorphic evolution of the southwest Yilgarn, in Accelerated Geoscience Program extended abstracts: Geological Survey of Western Australia, Record 2021/4, p. 108–115.

Korhonen, FJ, Kelsey, DE, Fielding IOH and Romano, SS 2020, The utility of the metamorphic rock record: constraining the pressure–temperature–time conditions of metamorphism: Geological Survey of Western Australia, Record 2020/14, 24p.

Pattison, DRM, Chacko, T, Farquhar, J and McFarlane, CRM 2003, Temperatures of granulite-facies metamorphism: constraints from experimental phase equilibria and thermobarometry corrected for retrograde exchange: Journal of Petrology, v. 44, no. 5, p. 867–900.

Pearce, MA, White, AJR and Gazley, MF 2015, TCInvestigator: automated calculation of mineral mode and composition contours for thermocalc pseudosections: Journal of Metamorphic Geology, v. 33, no. 4, p. 413–425, doi:10.1111/jmg.12126.

Pidgeon, RT, Wingate, MTD, Bodorkos, S and Nelson, DR 2010, The age distribution of detrital zircons in quartzites from the Toodyay – Lake Grace Domain, Western Australia: implications for the early evolution of the Yilgarn Craton: American Journal of Science, v. 310, p. 1115–1135.

Quentin de Gromard, R, Ivanic, TJ and Zibra, I 2021, Pre-Mesozoic interpreted bedrock geology of the southwest Yilgarn, 2021, *in* Accelerated Geoscience Program extended abstracts: Geological Survey of Western Australia, Record 2021/4, p. 122–144.

Powell, R and Holland, TJB 1988, An internally consistent dataset with uncertainties and correlations: 3. Applications to geobarometry, worked examples and a computer program: Journal of Metamorphic Geology, v. 6, no. 2, p. 173–204.

White, RW, Powell, R, Holland, TJB, Johnson, TE and Green, ECR 2014a, New mineral activity-composition relations for thermodynamic calculations in metapelitic systems: Journal of Metamorphic Geology, v. 32, no. 3, p. 261–286.

White, RW, Powell, R and Johnson, TE 2014b, The effect of Mn on mineral stability in metapelites revisited: New a–x relations for manganese-bearing minerals: Journal of Metamorphic Geology, doi:10.1111/jmg.12095.

Wilde, SA 2001, Jimperding and Chittering metamorphic belts, Western Australia — a field guide: Geological Survey of Western Australia, Record 2001/12, 24p.

Wingate, MTD, Bodorkos, S, and Kirkland, CL 2008a, 177901: quartzite, Kowalyou; Geochronology Record 739: Geological Survey of Western Australia, 5p.

Wingate, MTD, Bodorkos, S, and Kirkland, CL 2008b, 177904: quartzite, Windmill Hill; Geochronology Record 740: Geological Survey of Western Australia, 7p.

Wingate, MTD, Bodorkos, S, and Kirkland, CL 2008c, 177907: quartzite, Noondeening Hill; Geochronology Record 741: Geological Survey of Western Australia, 7p.

Wingate, MTD, Bodorkos, S, and Kirkland, CL 2008d, 177908: quartzite, Noondeening Hill; Geochronology Record 742: Geological Survey of Western Australia, 7p.

Links

Metamorphic history introduction document: Intro_2020.pdf

Appendix

EPMA compositional maps of garnet from sample 198520: garnet-bearing orthopyroxene pelitic granofels, Tregenza Road. Maps were analysed by energy-dispersive spectroscopy (EDS), and show relative elemental abundances. These garnet porphyroblasts were analysed from a thin section of the sample that is not part of the GSWA collection, and as such there is no information on mineral size or petrographic context; from Goscombe et al. (2015)

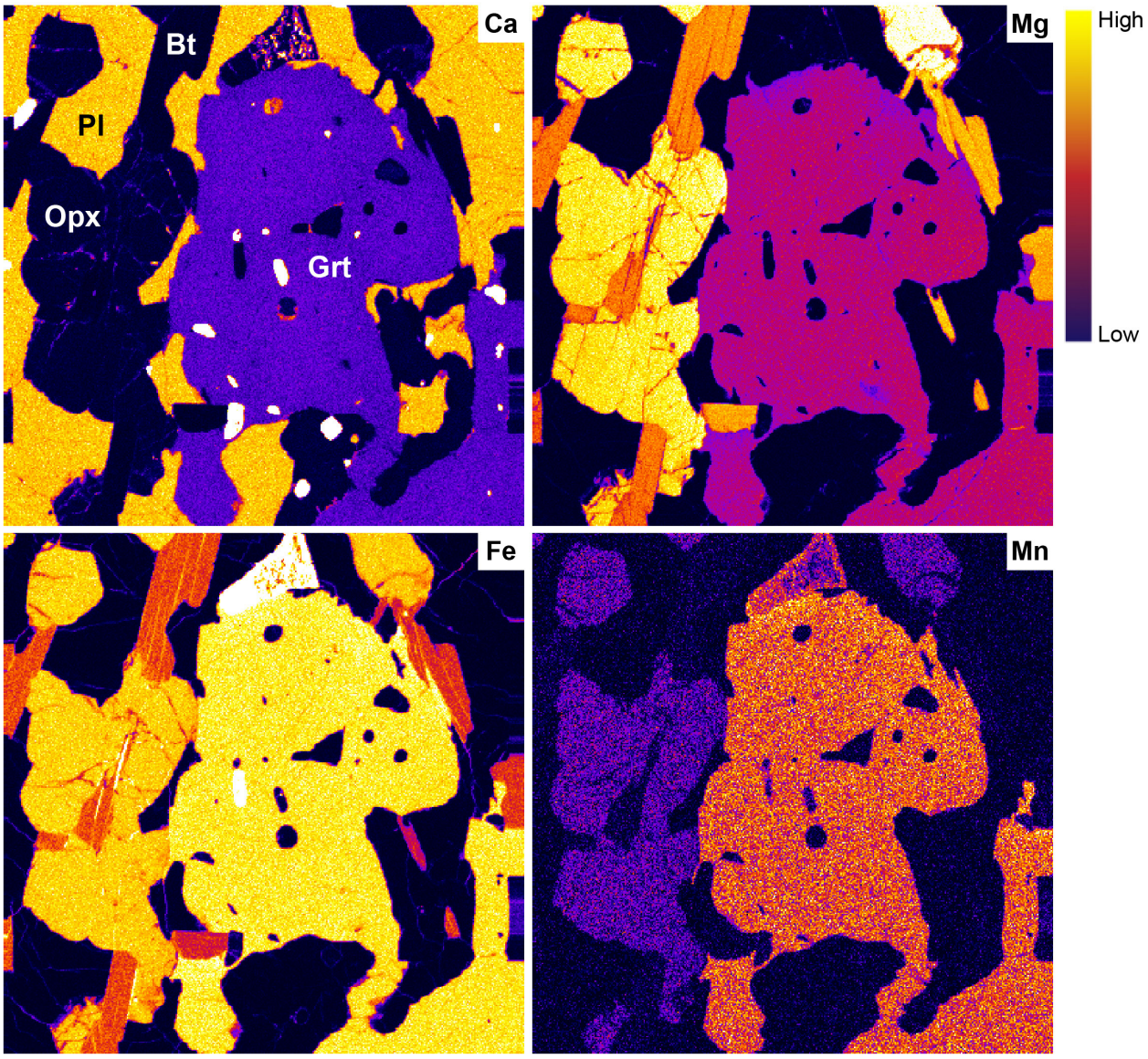

Recommended reference for this publication

Blereau, ER, Korhonen, FJ, Kelsey, DE and Fielding, IOH 2022, 198520: garnet-bearing orthopyroxene pelitic granofels, Tregenza Road; Metamorphic History Record 14: Geological Survey of Western Australia, 10p.

Data obtained: 19 May 2020

Date released: 14 April 2022

This Metamorphic History Record was last modified on 29 March 2022.

Grid references in this publication refer to the Geocentric Datum of Australia 1994 (GDA94). All locations are quoted to at least the nearest 100 m.

WAROX is GSWA's field observation and sample database. WAROX site IDs have the format 'ABCXXXnnnnnnSS', where ABC = geologist username, XXX = project or map code, nnnnnn = 6 digit site number, and SS = optional alphabetic suffix (maximum 2 characters).

Isotope and element analyses are routinely conducted using the GeoHistory laser ablation ICP-MS and Sensitive High-Resolution Ion Microprobe (SHRIMP) ion microprobe facilities at the John de Laeter Centre (JdLC), Curtin University, with the financial support of the Australian Research Council and AuScope National Collaborative Research Infrastructure Strategy (NCRIS). The TESCAN Integrated Mineral Analyser (TIMA) instrument was funded by a grant from the Australian Research Council (LE140100150) and is operated by the JdLC with the support of the Geological Survey of Western Australia, The University of Western Australia (UWA) and Murdoch University. Mineral analyses are routinely obtained using the electron probe microanalyser (EPMA) facilities at the Centre for Microscopy, Characterisation and Analysis at UWA, and at Adelaide Microscopy, University of Adelaide.

Digital data related to WA Geology Online, including geochronology and digital geology, are available online at the Department's Data and Software Centre and may be viewed in map context at GeoVIEW.WA.

Disclaimer
This product uses information from various sources. The Department of Mines, Industry Regulation and Safety (DMIRS) and the State cannot guarantee the accuracy, currency or completeness of the information. Neither the department nor the State of Western Australia nor any employee or agent of the department shall be responsible or liable for any loss, damage or injury arising from the use of or reliance on any information, data or advice (including incomplete, out of date, incorrect, inaccurate or misleading information, data or advice) expressed or implied in, or coming from, this publication or incorporated into it by reference, by any person whosoever.

© State of Western Australia (Department of Mines, Industry Regulation and Safety) 2022

With the exception of the Western Australian Coat of Arms and other logos, and where otherwise noted, these data are provided under a Creative Commons Attribution 4.0 International Licence. (http://creativecommons.org/licenses/by/4.0/legalcode)

Further details of geoscience products are available from:
Information Centre
Department of Mines, Industry Regulation and Safety
100 Plain Street
EAST PERTH WA 6004
Telephone: +61 8 9222 3459 | Email: publications@dmirs.wa.gov.au
www.dmirs.wa.gov.au/GSWApublications